TAM Kinases Promote Necroptosis by Regulating Oligomerization of MLKL

Graphical Abstract
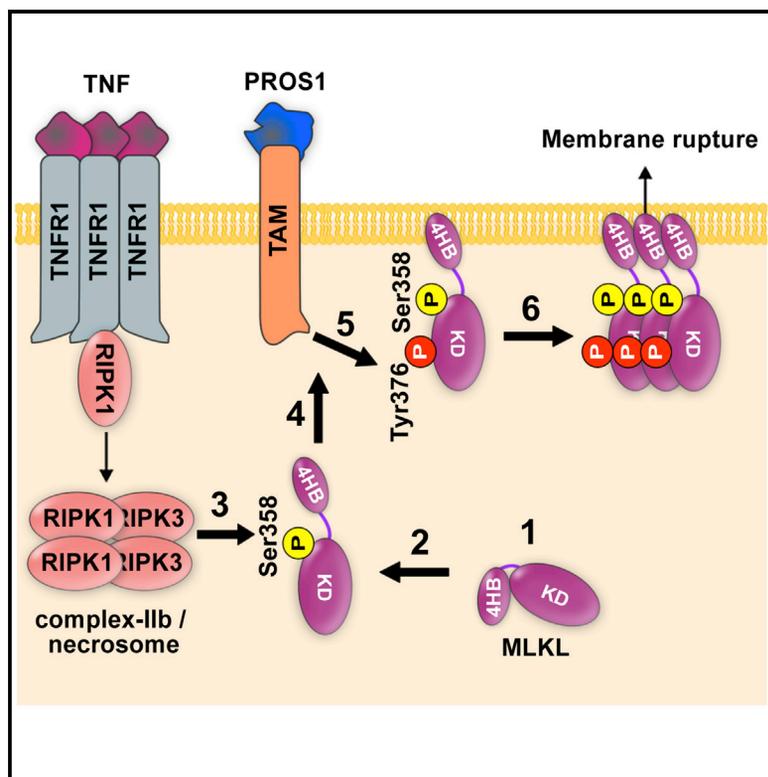
Authors

Ayaz Najafov, Adnan K. Mookhtiar, Hoang Son Luu, ..., Ying Li, Qingxian Lu, Junying Yuan

Correspondence

ayaz_najafov@hms.harvard.edu (A.N.), jyuan@hms.harvard.edu (J.Y.)

In Brief

TAM kinases are known for their oncogenic, anti-apoptotic, and anti-inflammatory roles. Najafov et al. discover an unexpected role for TAM kinases in mediating necroptosis, a pro-inflammatory programmed necrotic cell death. Mechanistic studies reveal that TAM kinases phosphorylate MLKL and promote its oligomerization, a step that forms a cell-membrane-rupturing pore.

Highlights

- TAM (Tyro3, Axl, and Mer) kinase activity is involved in mediating necroptosis

- TAM kinases phosphorylate MLKL to promote necroptosis

- TAM kinases mediate MLKL oligomerization to promote lytic pore formation

- TAM-null mice show resistance to systemic inflammatory response syndrome

CellPress

Molecular Cell

Article

CellPress

TAM Kinases Promote Necroptosis by Regulating Oligomerization of MLKL

Ayaz Najafov,[1,2,*] Adnan K. Mookhtiar,[1,2] Hoang Son Luu,[1] Alban Ordureau,[1] Heling Pan,[3] Palak P. Amin,[1,2] Ying Li,[3] Qingxian Lu,[4] and Junying Yuan[1,2,5,*]

[1]Department of Cell Biology, Harvard Medical School, Boston, MA 02115, USA
[2]Ludwig Center, Harvard Medical School, Boston, MA 02115, USA
[3]Interdisciplinary Research Center on Biology and Chemistry, Shanghai Institute of Organic Chemistry, Chinese Academy of Sciences, Shanghai 201210, China
[4]Department of Ophthalmology and Visual Sciences, University of Louisville School of Medicine, 301 E. Muhammad Ali Blvd., Louisville, KY 40202, USA
[5]Lead Contact
*Correspondence: ayaz_najafov@hms.harvard.edu (A.N.), jyuan@hms.harvard.edu (J.Y.)
https://doi.org/10.1016/j.molcel.2019.05.022

SUMMARY

Necroptosis, a cell death pathway mediated by the RIPK1-RIPK3-MLKL signaling cascade downstream of tumor necrosis factor α (TNF-α), has been implicated in many inflammatory diseases. Members of the TAM (Tyro3, Axl, and Mer) family of receptor tyrosine kinases are known for their anti-apoptotic, oncogenic, and anti-inflammatory roles. Here, we identify an unexpected role of TAM kinases as promoters of necroptosis, a pro-inflammatory necrotic cell death. Pharmacologic or genetic targeting of TAM kinases results in a potent inhibition of necroptotic death in various cellular models. We identify phosphorylation of MLKL Tyr376 as a direct point of input from TAM kinases into the necroptosis signaling. The oligomerization of MLKL, but not its membranal translocation or phosphorylation by RIPK3, is controlled by TAM kinases. Importantly, both knockout and inhibition of TAM kinases protect mice from systemic inflammatory response syndrome. In conclusion, this study discovers that immunosuppressant TAM kinases are promoters of pro-inflammatory necroptosis, shedding light on the biological complexity of the regulation of inflammation.

INTRODUCTION

Programmed cell death is a fundamental regulatory mechanism involved in regulating development, reproduction, immune defense, and tissue homeostasis of multicellular organisms (Yuan and Kroemer, 2010). Necroptosis is a recently discovered necrotic cell death pathway mediated by the RIPK1-RIPK3-MLKL signaling cascade downstream of tumor necrosis factor α (TNF-α), Fas, or TRAIL ligands, as well as downstream of Toll-like receptors (Christofferson and Yuan, 2010; Declercq

et al., 2009; Degterev et al., 2005; Kaiser et al., 2013; Murphy et al., 2013; Silke et al., 2015; Sun et al., 2012; Tait and Green, 2008; Wang et al., 2014). Cells are sensitized to necroptosis upon ablation of inhibitor of apoptosis proteins (IAPs; cIAP1, cIAP2, and XIAP) by Smac mimetics, such as SM-164 (Lu et al., 2008), as well as inhibition of caspases (e.g., the pan-caspase inhibitor zVAD.fmk).

Necroptosis requires the kinase activity of RIPK1 and RIPK3, which oligomerize to form the necrosome, resulting in RIPK3 activation (Cho et al., 2009; Li et al., 2012). Activated RIPK3 in turn phosphorylates the pseudokinase MLKL (Cho et al., 2009; He et al., 2009; Sun et al., 2012; Zhang et al., 2009). Phosphorylated MLKL forms an oligomeric, membrane-associated, channel-like structure that disrupts the integrity of the cell membrane and results in a lytic cell death (Hildebrand et al., 2014; Murphy et al., 2013; Pasparakis and Vandenabeele, 2015; Rickard et al., 2014; Tanzer et al., 2015; Wang et al., 2014).

Members of the TAM (Tyro3, Axl, and Mer) receptor family of tyrosine kinases activate multiple signaling cascades, including phosphatidylinositol-3 kinase (PI3K), p38 mitogen-activated protein kinase (MAPK), and Rac pathways, promoting cell growth, survival, and proliferation. They also play roles in regulation of inflammation and clearance of apoptotic cells (Lemke, 2013; Lemke and Rothlin, 2008; Lu and Lemke, 2001; Rothlin et al., 2007). TAM kinases are oncogenes, frequently amplified in a variety of cancers, where their overexpression correlates with poor patient survival (Janssen et al., 1991; Lai et al., 1994; Lemke, 2013; Linger et al., 2008; Lu and Lemke, 2001). Importantly, while TAM kinases are anti-apoptotic and established as important mediators of resolution of inflammation, their roles in necrotic and pro-inflammatory cell death are unknown.

In this study, we identify TAM kinases as key promoters of necroptosis signaling via regulation of the MLKL oligomerization step downstream of the necrosome.

RESULTS

TAM Kinases Are Required for Necroptotic Cell Death

Necroptosis has been recently linked to several inflammatory diseases. In order to elucidate novel components of the necroptosis
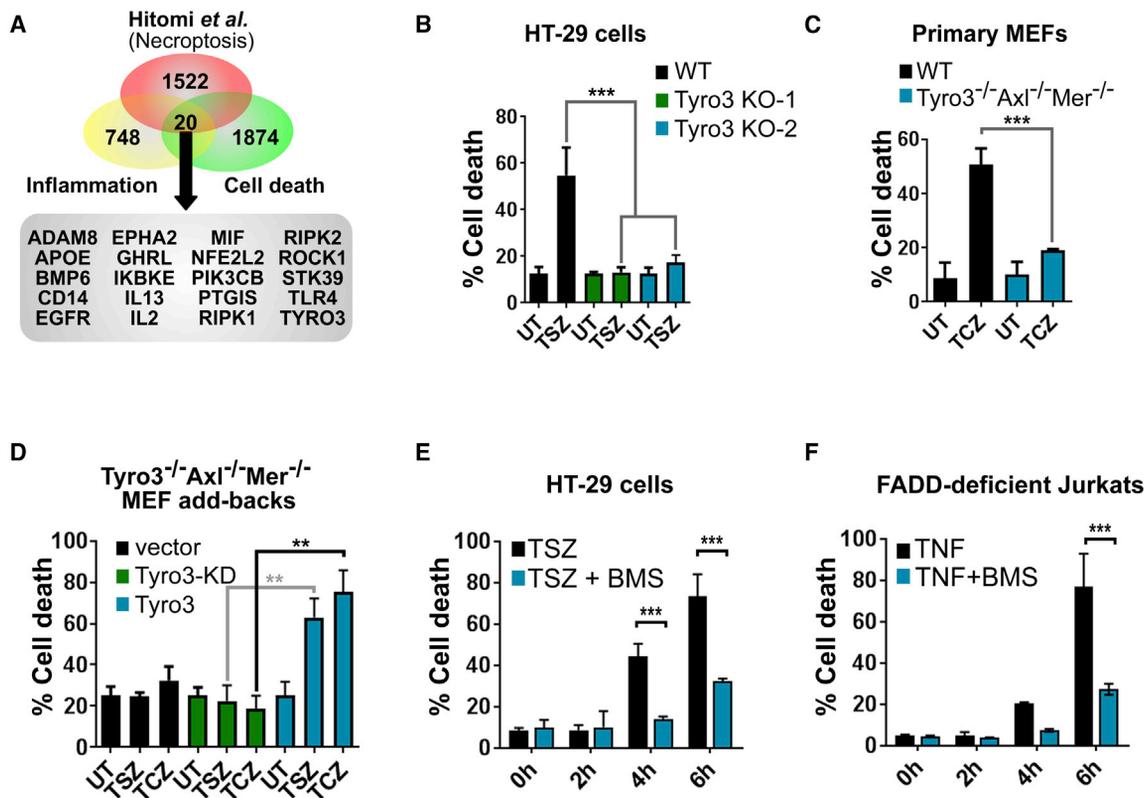
Figure 1. TAM Kinase Activity Mediates Necroptosis

(A) Bioinformatics analysis of genome-wide siRNA screen identifies Tyro3 as 1 of 20 putative mediators of necroptosis with known links to inflammation and cell death.

(B) CRISPR/Cas9-mediated knockout of Tyro3 in HT-29 cells (which do not express Axl or Mer) protects from TNF-α + SM-164 + zVAD.fmk (TSZ)-induced necroptotic cell death. Two different knockout clones were employed.

(C) Tyro3$^{-/-}$Axl$^{-/-}$Mertk$^{-/-}$ primary MEFs are resistant to TNF-α + CHX + zVAD.fmk (TCZ)-induced necroptosis.

(D) Reexpression of wild-type (WT), but not kinase-dead (KD; K540R), Tyro3 in immortalized Tyro3$^{-/-}$Axl$^{-/-}$Mertk$^{-/-}$ MEFs rescues resistance to TSZ- and TCZ-induced necroptotic cell death.

(E) Inhibition of TAM kinases by 10 μM BMS-777607 blocks TSZ-induced necroptosis in HT-29 cells.

(F) Inhibition of TAM kinases by 10 μM BMS-777607 blocks TNF-α-induced necroptosis in FADD-deficient Jurkat cells.

Cell death was quantified 16 h post-treatment, unless otherwise indicated, using membrane permeabilization-dependent Toxilight assay. One-way ANOVA was used. ***$p < 0.005$; **$p < 0.05$, Mean values ± SEM are shown. The experiments were repeated at least three times.

pathway that are linked to regulation of inflammation, we intersected our previously published data from a genome-wide necroptosis small interfering RNA (siRNA) screen (Hitomi et al., 2008) with the genome-wide list of genes known to play a role in the regulation of inflammation. We then narrowed down the candidate list by filtering out genes with no reported connection to regulation of cell death. This analysis yielded 20 hits, with Tyro3 as one of the top hits (Figure 1A).

We first confirmed the screen finding by siRNA-mediated knockdown of Tyro3 in HT-29 and L929 cells, which do not express Axl or Mer isoforms, using two different siRNA oligos. Knockdown of Tyro3 inhibited TSZ (TNF-α + SM-164 + zVAD.fmk)-induced necroptosis in HT-29 cells and necroptosis induced by either TNF-α or zVAD.fmk or their combination (TZ) in L929 cells (Figures S1A–S1C).

To determine the importance of TAM kinases for necroptotic cell death, we performed CRISPR/Cas9-mediated knockout of Tyro3 in HT-29 cells, which express relatively high levels of Tyro3 but low or no expression of Axl or Mer. We found that Tyro3-null HT-29 cells are resistant to necroptotic cell death, as no significant cell death induction was observed after 24-h TSZ treatment of two independent Tyro3-knockout (Tyro3^{KO}) HT-29 clones (Figures 1B and S1A). Consistently, both primary and immortalized Tyro3$^{-/-}$Axl$^{-/-}$Mer$^{-/-}$ mouse embryonic fibroblasts (MEFs) were resistant to TSZ- and TCZ (TNF-α + cycloheximide + zVAD.fmk)-induced necroptosis (Figures 1C and S1D). Notably, Tyro3$^{-/-}$Axl$^{+/-}$Mer$^{-/-}$ MEFs were only partially protected from these necroptosis stimuli, suggesting that Axl expression is sufficient to mediate the necroptosis signaling, in the absence of Tyro3 and Mer expression (Figure S1E). Moreover, expression of Tyro3, Axl, or Mer in the Tyro3$^{-/-}$Axl$^{-/-}$Mer$^{-/-}$ MEFs was sufficient to rescue the resistance of these cells to necroptosis (Figure S1F). On the other hand, Tyro3$^{-/-}$Axl$^{-/-}$Mer$^{-/-}$ MEFs were not significantly protected from TNF-α + cycloheximide (CHX)-induced apoptosis (Figure S1G).
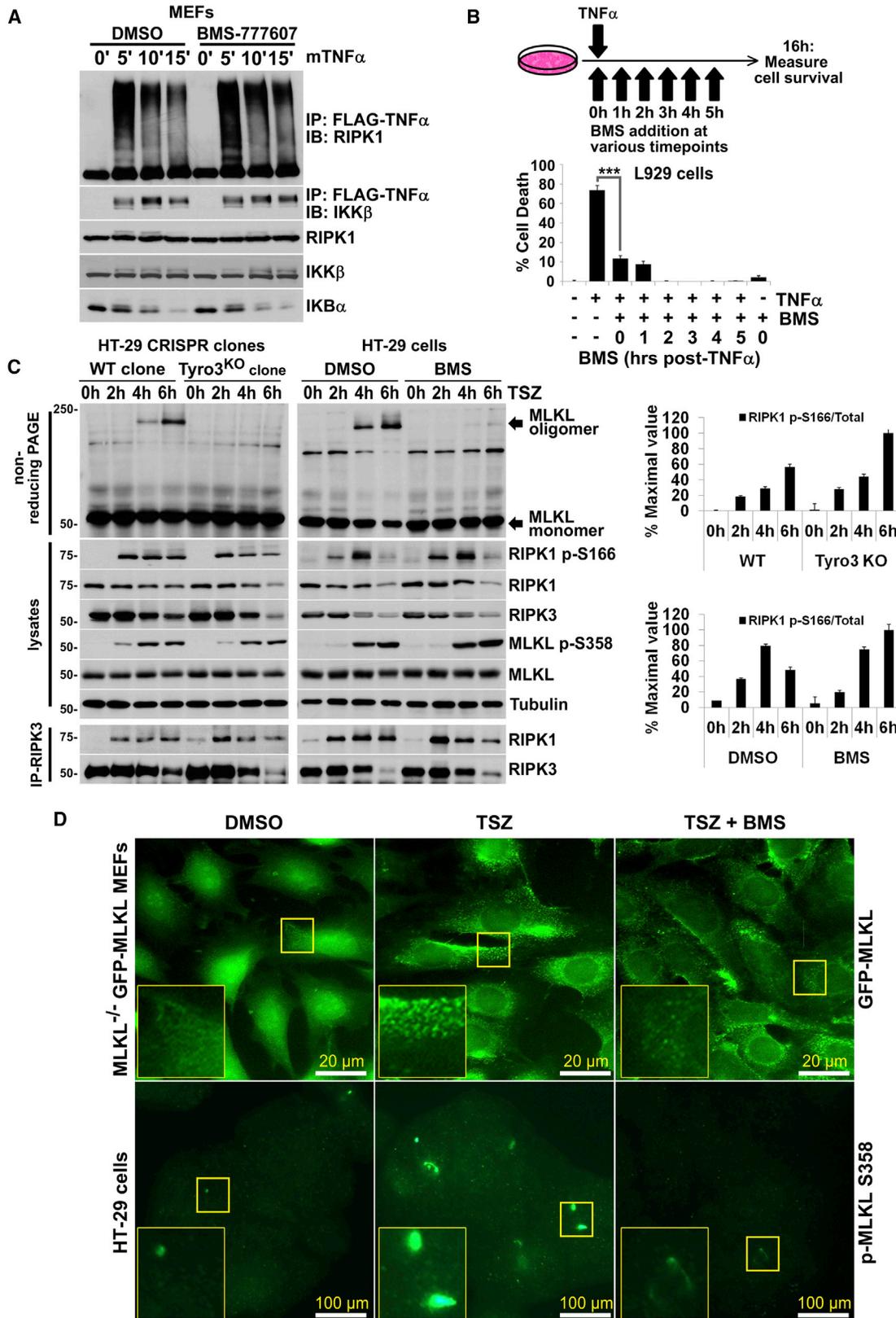
(legend on next page)

Notably, reexpression (add-back) of wild-type, but not kinase-dead, Tyro3-FLAG from an ectopically expressed plasmid restored the sensitivity of TAM-null MEFs to necroptosis (Figure 1D). A similar observation was made when Tyro3-FLAG was reexpressed in Tyro3^{KO} HT-29 cells (Figure S1H). On the other hand, further increasing total Tyro3 protein levels (on top of endogenous levels) by stable overexpression of Tyro3-FLAG plasmid in L929 cells resulted in sensitization to TNF-α-induced necroptosis (Figure S1I).

Concordant with the knockout data, the TAM kinase inhibitor BMS-777607 (BMS) potently blocked TSZ-induced necroptosis in HT-29 cells (Figure 1E) and TNF-α-induced necroptosis in FADD-deficient Jurkat cells (Figure 1F), as well as necroptosis in L929 cells induced by TNF-α, zVAD.fmk, or TZ (Figures S2A–S2D) and TSZ or TCZ-induced necroptosis in MEFs (Figures S2E and S2F). Importantly, the inhibitory effect of BMS-777607 on necroptosis was blocked by expression of a BMS-777607-resistant "gatekeeper" mutant of Tyro3 (Ala672Thr), confirming the specificity of the compound in our experiments (Figure S2G).

Moreover, we employed LDC1267, a structurally distinct (to BMS-777607), potent, and selective inhibitor of TAM kinases (Paolino et al., 2014), and found a significant and dose-dependent inhibition of TNF-α-induced necroptosis in L929 cells and TSZ-induced necroptosis in HT-29 cells upon pretreatment with this compound (Figures S2H and S2I)

Overall, these results provide strong evidence that the activity of TAM kinases is required for necroptosis.

TAM Kinases Regulate the Necroptosis Pathway Downstream of the Necrosome and Upstream of MLKL Oligomerization

The inhibition of TAM kinases did not block complex I, as determined by RIPK1 ubiquitination and IκBα degradation following 5–15 min of TNF-α treatment of wild-type MEFs (Figure 2A). Moreover, we ruled out the involvement of TAM kinases in complex I, with regards to protection from necroptosis, by performing a delayed BMS-777607 treatment (after complex-I resolution), which still resulted in inhibition necroptotic cell death (Figure 2B).

Knockout or inhibition of TAM kinases also did not inhibit necrosome formation, as measured by RIPK1/RIPK3 association in IP-RIPK3 experiments and RIPK3 phosphorylation at Ser227 following TSZ treatment of HT-29 cells (Figures 2C and S3A). Moreover, phosphorylation of MLKL at Ser358 (RIPK3 site) was

also not inhibited (Figures 2C and S3B). Finally, the membrane translocation of MLKL was also not inhibited by BMS-777607 (Figure S3C). On the other hand, MLKL oligomerization was significantly inhibited upon knockout and inhibition of TAM kinases, as determined by non-reducing PAGE and fluorescence microscopy (Figures 2C and 2D). These experiments establish that TAM kinase inhibition results in the blocked necroptotic cell death due an input point located downstream of the necrosome and upstream of MLKL oligomerization.

TAM Kinases Directly Regulate MLKL Oligomerization

In order to show that TAM kinases regulate MLKL directly, we employed a constitutively active (RIPK3-independent) MLKL mutant, Q356A, that oligomerizes and kills cells upon its expression (Murphy et al., 2013). We generated a stable cell line with doxycycline-inducible expression of MLKL^{Q356A} using the isogenic HEK293-Flp-In-T-Rex system. Strikingly, TAM kinase inhibition (Figures 3A, 3B, and S3D), as well as knockout (Figure 3C), resulted in reduction of MLKL^{Q356A} oligomerization and protected from MLKL^{Q356A}-induced lytic cell death. Notably, this was phenocopied using transient transfection of MLKL^{Q356A} into TAM-null MEFs (Figure 3D). Similar results were obtained using mouse MLKL^{Q343A} and human MLKL$^{T357E and S358D}$ constitutively active mutants (Figures S3E–S3G).

On the other hand, PI3K inhibition by GDC-0941 had no effect on MLKL oligomerization or cell death, ruling out a potential input from the TAM kinase-PI3K cascade (Figure 3A). The MLKL membranal translocation inhibitor necrosulfonamide (NSA) inhibited MLKL^{Q356A}-induced cell death but did not inhibit MLKL oligomerization, suggesting that the membranal translocation and oligomerization are distinct steps in MLKL activation and function (Figure 3A).

Tyro3 knockdown also protected from MLKL^{Q356A}-induced cell death (Figure S3H), while overexpression of Tyro3 sensitized cells to it (Figure S3H). Sensitization to cell death induced by mouse MLKL^{Q343A} constitutively active mutant was obtained when Tyro3, Axl, or Mer was overexpressed (Figure S3J). These findings strongly suggest that TAM kinases regulate MLKL directly.

TAM Kinases Directly Phosphorylate MLKL during Activation of Necroptosis

Next, we tested the potential physical interaction between TAM kinases and MLKL using various pull-down approaches

Figure 2. TAM Kinases Regulate the Necroptosis Signaling Pathway Downstream of the Necrosome

(A) Complex I is not blocked by the TAM kinase inhibitor BMS-777607 in MEFs. Cells were treated with 100 ng/mL FLAG-mTNF-α, and complex I was immunoprecipitated using anti-FLAG-agarose beads. Cell lysates were immunoblotted with the indicated antibodies. The experiment was repeated two times.

(B) Treatment of L929 cells with the TAM kinase inhibitor BMS-777607 after resolution of complex I still results in protection from TNF-α-induced necroptosis. 10 μM BMS-777607 was added to the medium at the indicated time points following TNF-α treatment, and cell survival was measured 16 h later. Cell death was quantified using the membrane-permeabilization-dependent Toxilight assay. Mean values ± SEM are shown. The experiment was repeated at least three times.

(C) Effect of knockout (left panel) and inhibition (right panel) of TAM kinases in HT-29 cells on necroptosis signaling. RIPK1-RIPK3 interaction and p-MLKL (Ser358) are not significantly inhibited, while MLKL oligomerization is reduced. Cell lysates were resolved on either non-reducing PAGE (top panel) or SDS-PAGE (middle panel) or subjected to IP-RIPK3 (lower panel). Immunoblotting was done using indicated antibodies. The quantification of the RIPK1 p-Ser166 levels with respect to total RIPK1 levels is shown as a percentage of maximal values in each dataset. The experiment was repeated three times.

(D) BMS-777607 blocks TSZ-induced GFP-MLKL oligomerization in MEFs, as judged by fluorescence microscopy, and oligomerization of endogenous MLKL in HT-29 cells, as judged by immunofluorescence microscopy analysis using p-MLKL S358 antibody. Note that since p-MLKL S358 levels are not decreased by BMS-777607 (Figure 2C), this immunostaining is expected to reflect the MLKL oligomerization levels. Cells were treated with TSZ for 5 h ± 10 μM BMS-777607 and fixed with 4% paraformaldehyde. The experiment was repeated two times.
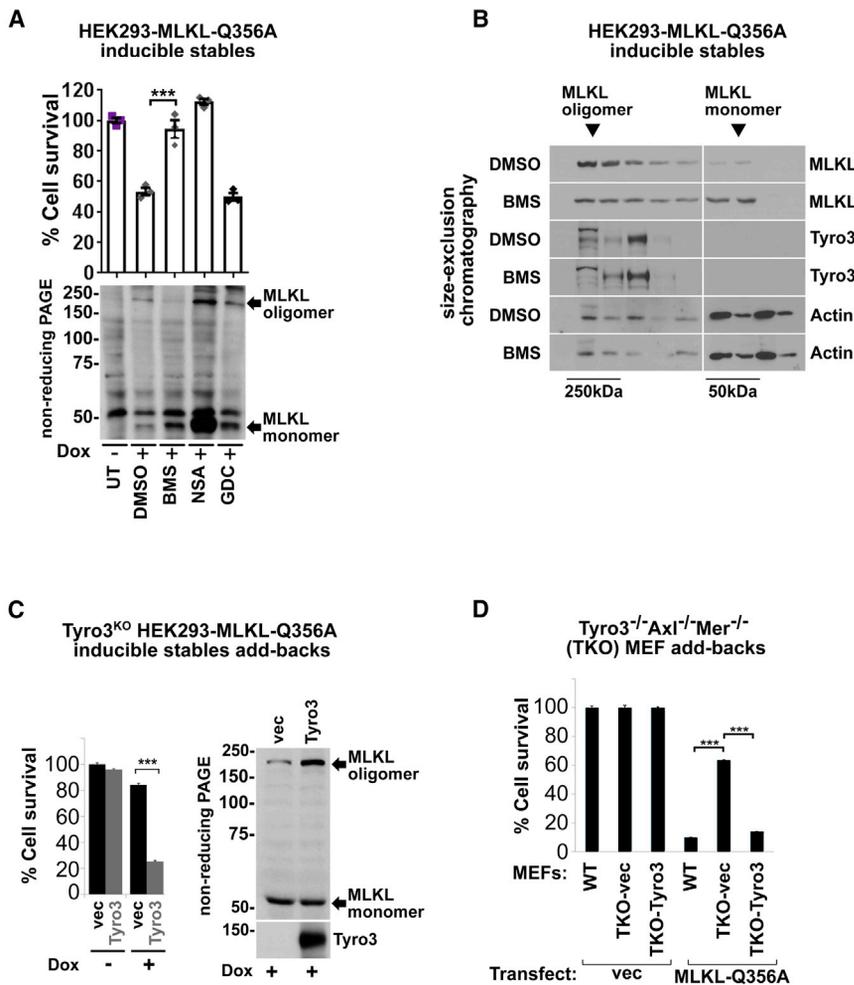
Figure 3. TAM Kinases Regulate the Necroptosis Signaling Pathway via MLKL Oligomerization

(A) BMS-777607, but not necrosulfonamide or GDC-0941, blocks oligomerization of constitutively active MLKL^{Q356A} mutant and protects cells from necroptotic cell death. HEK293-Flp-In-Trex-hMLKL^{Q356A} cells were treated with 0.5 μg/mL doxycycline for 16 h in the presence of the indicated compounds, and cell survival was measured using the CellTiterGlo assay. Cell lysates were resolved on non-reducing PAGE and immunoblotted for MLKL. DMSO, vehicle; BMS, BMS-777607 (10 μM); NSA, necrosulfonamide (1 μM); GDC, PI3K inhibitor GDC-0941 (1 μM). The experiment was repeated three times.

(B) As in (A), except cell lysates were fractionated by size-exclusion chromatography following 8 h of doxycycline treatment and fractions were immunoblotted with the indicated antibodies. The experiment was repeated two times.

(C) TAM kinase knockout in HEK293 cells protects from necroptotic cell death induced by constitutively active MLKL^{Q356A} mutant expression and its oligomerization. Tyro3^{KO} HEK293-Flp-In-Trex-hMLKL^{Q356A} cells (do not express Axl or Mer) complemented with either empty vector (vec) or Tyro3-FLAG plasmid (Tyro3) were treated with 0.2 μg/mL doxycycline and analyzed for cell death and MLKL oligomerization as in (A) 16 hr later. The experiment was repeated three times.

(D) TAM kinase triple knockout in MEFs protects from necroptotic cell death induced by constitutively active MLKL^{Q356A} mutant expression. Empty vector or constitutively active MLKL^{Q356A} mutant was transiently transfected into either wild-type (WT) or indicated Tyro3$^{-/-}$Axl$^{-/-}$Mertk$^{-/-}$ MEFs complemented with either empty vector (TKO-vec) or Tyro3-FLAG plasmid (TKO-Tyro3). Cell survival was measured 24 h later using the CellTiterGlo assay. The experiment was repeated three times.
***p < 0.005, Mean values ± SEM are shown.

(Figures 4A–4D). We found that endogenous Tyro3 and Axl interacted with endogenous MLKL after treatment of HeLa-GFP-RIPK3 cells with TSZ for 4 h (Figure 4A). TNF-α-induced necroptosis resulted in interaction of endogenous MLKL with Tyro3-FLAG stably expressed in L929 cells (Figure 4B). Similarly, TSZ treatment induced interaction of endogenous Tyro3 with MLKL-FLAG stably expressed at near-endogenous levels in MLKL^{KO} HT-29 cells (Figure 4C). Additionally, MLKL^{Q356A} interacted with endogenous Tyro3 in HEK293 cells (Figure 4D) and endogenous MLKL interacted with endogenous Mer in FADD-deficient Jurkat (FDJ) cells following TNF-α treatment for 4 h (Figure S4A). These results indicate that all three TAM kinase family members can interact with MLKL during necroptosis.

Remarkably, purified Tyro3 robustly phosphorylated purified MLKL *in vitro*, upon which MLKL oligomerized (Figures 4E and S4B). Importantly, we found that TSZ treatment of HT-29 cells resulted in tyrosine phosphorylation of MLKL, as judged by anti-phospho-tyrosine antibody, and BMS-777607 treatment blocked this induction and concomitant oligomerization (Fig-

ure 4F). Phos-tag analysis also revealed that some of the endogenous MLKL phosphorylation events induced by TSZ treatment of HT-29 cells were blocked by BMS-777607 (Figure S4C). This is also consistent with our observation that Ser358 phosphorylation of MLKL is not blocked by BMS-777607 (Figure 2C).

We performed *in vitro* and *in vivo* phosphomapping experiments to determine which MLKL tyrosine residues are phosphorylated by TAM kinases directly, as well as during necroptosis (Figures 4G and 4H). Mass spectrometry analysis revealed that several MLKL tyrosine (Tyr) residues (Tyr222, Tyr343, Tyr376, and Tyr389) are phosphorylated by Tyro3 *in vitro* (Figures 4G and S4D), while the *in vivo* Tyr phosphorylation following TSZ treatment was revealed to be at Tyr376 (Figures 4H and S4D). These four Tyr residues are all strongly conserved across species, suggesting a potential importance in their function (Figure S4E). Interestingly, Tyr343 and Tyr389 are located in close proximity to the MLKL activation loop (T-loop) and the RIPK3 site Ser358 (Figure S4E). Moreover, Tyr376 is located in the MLKL T-loop itself, just before the "APE" kinase motif, suggesting that the phosphorylation of

A HeLa-GFP-RIPK3 cells

UT TSZ-4h

lysates: TYRO3, MLKL | AXL, MLKL

IP: MLKL: TYRO3, MLKL | AXL, MLKL

B L929 stables

vector | Tyro3-Flag

TNF (6hrs): - + - +

lysates: Tyro3, MLKL

IP: FLAG: Tyro3, MLKL

C MLKL^{KO} HT-29 add-backs

vector | MLKL-Flag

0h 2h 4h 6h 0h 2h 4h 6h TSZ (hrs)

lysates: Tyro3, MLKL

IP: FLAG: Tyro3, MLKL

D HEK293-MLKL-Q356A inducible stables

- + Dox

lysates: Tyro3, MLKL

IP: FLAG: Tyro3, MLKL

E *in vitro* kinase assay

- + + + MLKL
+ - + + Tyro3
- - - + BMS

^{32}P, CBB — MLKL
^{32}P, CBB — Tyro3

non-reducing PAGE
250-
MLKL oligomer
50-
MLKL monomer

F MLKL^{KO} MLKL-Flag HT-29 add-backs

TSZ - + +
BMS - - +

50- p-Tyr
50- MLKL

non-reducing PAGE
250-
MLKL oligomer
50-
MLKL monomer

High exposure | Low exposure
IP: Flag

G *in vitro* phosphomapping

Transfect Tyro3-Flag
HEK293T cells
48h: Harvest, IP-Flag → Elute

Transfect GST-MLKL | 47h: Add BMS
HEK293T cells
48h: Harvest, GST-pull-down → Elute

→ *in vitro* kinase reaction ± BMS

SDS-PAGE, Cut out MLKL bands

Mass Spec:
Ⓟ Tyr222
Ⓟ Tyr343
Ⓟ Tyr376
Ⓟ Tyr389

H *in vivo* phosphomapping

MLKL$^{-/-}$ MLKL-Flag HT-29 add-backs
TSZ → 2h: DMSO / BMS → SDS-PAGE, Cut out MLKL bands
5h: Harvest, IP-Flag
Mass Spec: Ⓟ Tyr376

I HEK293-MLKL-Q356A inducible stables

% Cell death
120
100
80 ***
60
40
20
0
Q356A | Q356A Y376F

non-reducing PAGE
Q356A | Q356A Y376F
250-
MLKL oligomer
50-
MLKL monomer

J HT-29 cells

- + + + TSZ (4h)
- - + - BMS (10 µM)
- - - + LDC (20 µM)

IP: p-MLKL Tyr376
IB: MLKL

MLKL (Lysates)

(legend on next page)

Tyr376 may involve regulation of functions related to MLKL T-loop phosphorylation by RIPK3 at Ser358.

Importantly, Tyr376Phe-phosphorylation-resistant mutation blocked MLKL^{Q356A} oligomerization and necrotic cell death (Figure 4I). We have confirmed that the MLKL$^{Q356A;Y376F}$ mutant is not misfolded by assessing its solubility (Figure S4F), as well as sensitivity to proteolysis in lysates, demonstrating that unlike degradation-sensitive IκBα, both MLKL^{Q356A} and MLKL$^{Q356A;Y376F}$ mutants are resistant to degradation (Figure S4G).

Finally, we developed a p-Tyr376 MLKL antibody (Figure S4H) and found that endogenous MLKL is phosphorylated at this residue following necroptosis activation in HT-29 cells in a TAM kinase-dependent manner, consistent with the mass spectrometry data (Figure 4J). This antibody was not suitable for western blotting but performed well for immunoprecipitation experiments (Figure 4J). Moreover, stable expression of wild type, but not Tyr376Phe mutant of MLKL, resulted in regain of sensitivity to TSZ-induced necroptosis in MLKL^{KO} HT-29 cells (Figures S4I and S4J). Finally, unlike MLKL^{WT}, MLKL^{Y376F}, expressed in MLKL^{KO} HT-29 cells, did not oligomerize following TSZ treatment (Figure S4K). These results suggest that TAM kinases phosphorylate MLKL kinase domain (KD) at Tyr376 during necroptosis, promoting its oligomerization, consistent with the report that the MLKL KD is involved in the regulation of its oligomerization (Tanzer et al., 2016).

We next investigated how the MLKL and Tyro3 interaction is regulated. Interestingly, while N-terminally glutathione S-transferase (GST)-tagged full-length MLKL interacted with endogenous Tyro3 upon overexpression in HEK293T cells (Figure S5A), C-terminally FLAG-tagged MLKL interacted under the same conditions only upon deletion of the 4HB domain (Δ[1–181]), suggesting that the MLKL-Tyro3 interaction is inhibited by the 4HB domain and that the MLKL KD binds to Tyro3 (Figure S5B).

The Δ[1–181] fragment of MLKL was phosphorylated at Tyr376 upon overexpression of Tyro3 in HEK293T cells, indicating that the 4HB domain, and therefore the binding of MLKL to the plasma membrane, is not required for MLKL's interaction with TAM kinases in cells (Figure S5C). Consistent with this notion and the observation that MLKL oligomerization is not blocked by NSA (shown in Figure 3A and by Wang et al., 2014), NSA treatment partially decreased but did not block MLKL Tyr376 phosphorylation following TSZ treatment (Figure S5D). Additionally, TAM-kinase-induced oligomerization of MLKL in vitro also did not require the 4HB domain or lipid presence (Figure S5E).

These findings strongly suggest that both MLKL oligomerization and necrotic cell death depend on MLKL phosphorylation by TAM kinases, at least at Tyr376, and that the 4HB domain of MLKL could be impinging on the interaction between TAM kinases and the KD of MLKL This negative regulation may be alleviated by RIPK3 phosphorylation of MLKL at Ser358, as well as deletion of the 4HB domain. In the context of the published negative effect of the MLKL KD on the ability of the 4HB domain to bind to lipids (Hildebrand et al., 2014; Wang et al., 2014), our data provide evidence for a dual-autoinhibition mechanism that keeps MLKL in its inactive state, unable to bind to the

Figure 4. MLKL Is a Direct Target of TAM Kinases during Activation of Necroptosis

(A) Endogenous Tyro3 and Axl interact with endogenous MLKL in HeLa-GFP-RIPK3 cells after TSZ-induced necroptosis. Cells were treated for 4 h, and MLKL immunoprecipitates and lysates were immunoblotted with the indicated antibodies. The experiment was repeated two times.

(B) Endogenous MLKL interacts with Tyro3-FLAG upon 6-h TNF-α treatment of L929 cells stably expressing Tyro3-FLAG. Anti-FLAG-agarose immunoprecipitates (eluted with FLAG peptide) and cell lysates were immunoblotted with indicated antibodies. The experiment was repeated two times.

(C) Endogenous Tyro3 interacts with MLKL-FLAG upon TSZ treatment of HT-29-MLKL-FLAG (MLKL knockout cells that stably reexpress MLKL-FLAG at near-endogenous levels) for the indicated time points. Anti-FLAG-agarose immunoprecipitates (eluted with FLAG peptide) and cell lysates were immunoblotted with indicated antibodies.

(D) Constitutively active MLKL^{Q356A} interacts with endogenous Tyro3. HEK293-Flp-In-Trex-hMLKL^{Q356A} cells were treated with 0.2 μg/mL doxycycline for 8 h, and cell lysates were subjected to anti-FLAG pull-down. Cell lysates and anti-FLAG immunoprecipitates (eluted with FLAG peptide) were immunoblotted with the indicated antibodies. The experiment was repeated two times.

(E) Purified Tyro3 phosphorylates purified MLKL and induces its oligomerization. An in vitro kinase assay using ^{32}P-γ-ATP shows direct phosphorylation of GST-MLKL-FLAG by Tyro3, which is blocked by the TAM kinase inhibitor BMS-777607 used at 3 μM. Hot or cold reactions were resolved on non-reducing PAGE and immunoblotted with the indicated antibodies. C-terminally FLAG-tagged MLKL was used for the non-reducing PAGE experiment. Asterisks indicate the nonspecific band from Tyro3 fragment autophosphorylation. ^{32}P, autoradiography; CBB, Coomassie brilliant blue staining of purified MLKL bands. The experiment was repeated two times.

(F) TAM kinases phosphorylate MLKL during necroptosis and induce its oligomerization. MLKL^{KO} HT-29 cells stably expressing MLKL-FLAG were treated with TSZ for 6 h $\pm$ 10 μM BMS-777607, and anti-FLAG-agarose immunoprecipitates were eluted with FLAG peptide and immunoblotted with the indicated antibodies after resolving on either SDS-PAGE or non-reducing PAGE. The experiment was repeated two times.

(G) Outline of the in vitro phosphomapping experiment. HEK293T cells were transiently transfected with either Tyro3-FLAG or GST-MLKL, and proteins were purified separately. BMS-777607 was added to cells expressing GST-MLKL 1 h prior to harvesting (47th h) in order to eliminate background phosphorylation of GST-MLKL by endogenous TAM kinases due to overexpression of GST-MLKL. Following an in vitro kinase assay employing the purified Tyro3-FLAG and GST-MLKL in the presence or absence of TAM kinase inhibitor BMS-777607, MLKL bands were cut out of SDS-PAGE and analyzed by mass spectrometry. The indicated Tyr residues were found to be phosphorylated only in the absence of BMS-777607 in the in vitro reaction.

(H) Outline of the in vivo phosphomapping experiment. MLKL^{KO} HT-29 cells stably expressing MLKL-FLAG were treated with TSZ for 6 h $\pm$ BMS-777607, and anti-FLAG-agarose immunoprecipitates were resolved on SDS-PAGE. MLKL bands were cut out of the gel and analyzed by mass spectrometry. Tyr376 was found to be phosphorylated following TSZ treatment in the absence of BMS-777607.

(I) Mutation of Tyr376 to phosphorylation-resistant Phe blocks necrotic cell death induced by constitutively active MLKL^{Q356A}. HEK293-Flp-In-Trex-hMLKL^{Q356A} cells were treated with 0.5 μg/mL doxycycline for 16 h, and cell survival was measured using the CellTiterGlo assay. Cell lysates were resolved on non-reducing PAGE and immunoblotted for MLKL. The experiment was repeated two times. ***$p < 0.005$, Mean values $\pm$ SEM are shown.

(J) MLKL is phosphorylated at Tyr376 in a TAM kinase-dependent manner. HT-29 cells were treated with TSZ for 4 h in the presence or absence of TAM kinase inhibitors BMS-777607 (10 μM) or LDC1267 (20 μM) and endogenous MLKL was immunoprecipitated using anti-phospho-Tyr376 antibody. The immunoprecipitates and lysates were immunoblotted for MLKL.

CellPress
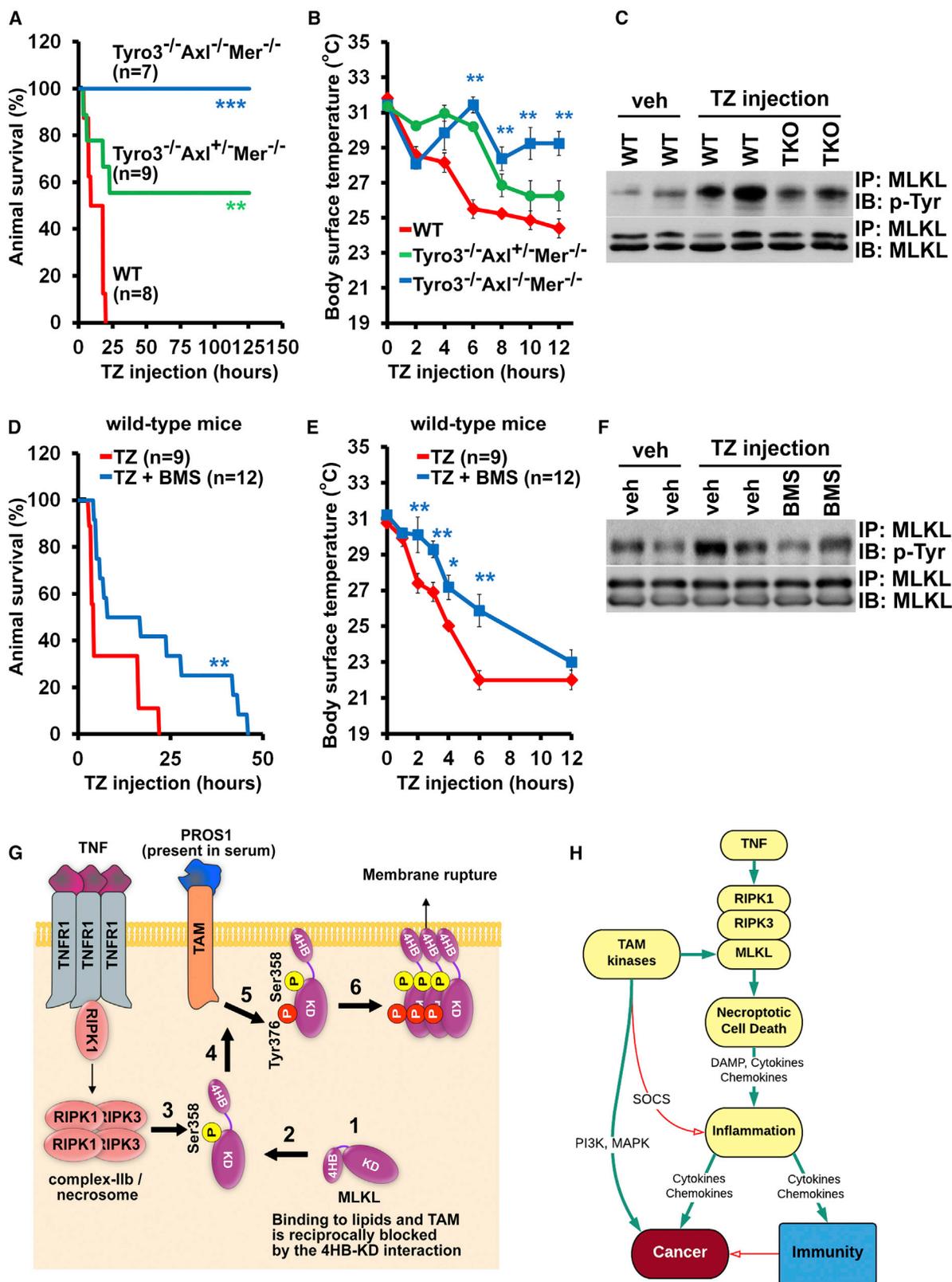
plasma membrane via its 4HB domain or TAM kinases via its KD in the absence of RIPK3 activation (Figure S5F).

Importantly, according to the published crystal structures of the inactive MLKL conformation (Murphy et al., 2013, 2014), Tyr376 residue is not exposed to the solvent and is facing the internal moiety of the pseudokinase domain. This would be consistent with our model that TAM kinases, which are active under basal conditions (while MLKL is in its inactive conformation), phosphorylate MLKL only during necroptosis activation, when MLKL is in its active conformation, due to phosphorylation by RIPK3.

Tyr376 is located in the T-loop region of MLKL, two residues N-terminal to the protein kinase APE motif (APE^{-2}) (which is SPQ for human MLKL). To inquire about the importance of the phosphorylation of Tyr residues at this position in protein KDs, we analyzed amino acid (http://kinase.com) (Manning et al., 2002) and phosphorylation databases (https://www.phosphosite.org/) (Hornbeck et al., 2015) to reveal how prevalent such phosphorylation is in the kinome. We found that out of 516 kinases analyzed, 138 kinases (26.7%) have a Tyr residue the APE^{-2} position (Figure S5G), and the Tyr residues in 43 (31.1%) of these kinases has been reported to be phosphorylated (Figure S5H).

Kinome tree analysis (http://kinhub.org) (Eid et al., 2017) revealed that phosphorylated APE^{-2} Tyr residues are found in various kinase families, including the tyrosine-kinase-like (TKL) family, to which MLKL belongs (Figures S5I and S5J).

Thus, it is likely that Tyr376 is internal prior to RIPK3 phosphorylation; following the phosphorylation of the adjacent T-loop residues (Ser357 and 358) and opening of the MLKL kinase conformation, Tyr376 is exposed and can be phosphorylated by TAM kinases. Accordingly, Tyr376 being always exposed to the solvent would be inconsistent with the proposed model, since TAM kinases would be able to phosphorylate it under basal conditions, which would lead to MLKL oligomerization without necroptosis stimuli.

TAM Kinases Are Essential for Systemic Inflammatory Response Syndrome

Necroptosis plays an important role in TZ-induced systemic inflammatory response syndrome (SIRS), as both RIPK3$^{-/-}$ and MLKL$^{-/-}$ mice are protected from it (Duprez et al., 2011; Newton et al., 2016). Remarkably, Tyro3$^{-/-}$Axl$^{-/-}$Mertk$^{-/-}$ mice were completely resistant to the SIRS-induced death (Figure 5A) and quickly recovered from hypothermia (Figure 5B), similar to RIPK3$^{-/-}$ mice (Duprez et al., 2011; Newton et al., 2016), while Tyro3$^{-/-}$Axl$^{+/-}$Mertk$^{-/-}$ mice showed partial protection. Since mouse liver tissue undergoes a significant amount of cell death following TZ-induced SIRS (Duprez et al., 2011), we analyzed MLKL Tyr phosphorylation in this tissue following TZ injections. Importantly, SIRS robustly induced Tyr phosphorylation of MLKL in mouse livers, which was potently inhibited in Tyro3$^{-/-}$Axl$^{-/-}$Mertk$^{-/-}$ livers (Figure 5C).

We employed BMS-777607 to confirm these SIRS findings obtained with the TAM-null mice. Notably, despite having a half-life of ~4.5 h in vivo (Schroeder et al., 2009), BMS-777607 injections significantly improved mouse survival and hypothermia following TZ-induced SIRS (Figures 5D and 5E) and also inhibited TZ-induced MLKL Tyr phosphorylation (Figure 5F). Together, these findings highlight the important role of TAM kinases in mediating SIRS and promoting MLKL phosphorylation during necroptosis induction by TZ in vivo.

DISCUSSION

We identify TAM kinases as novel regulators of necroptosis and MLKL oligomerization (Figure 5G). In the absence of pro-necroptosis stimuli, the 4HB domain of MLKL interacts with the KD and is unable to bind to the plasma membrane phospholipids, while this interaction also renders the KD unable to bind to the TAM kinases, which are active under basal conditions, due to the presence of their PROS1 ligand in the serum (Figure 5G, step 1). During necroptosis activation, MLKL is recruited to the complex IIb also known as necrosome (Figure 5G, step 2) and gets phosphorylated at Ser358 by RIPK3 (Figure 5G, step 3). This phosphorylation results in dislocation of the 4HB domain away from the KD, resulting in de-repression of the lipid-binding capacity of the 4HB domain (Hildebrand et al., 2014; Wang et al., 2014) and de-repression of the TAM-kinase-binding capacity of the KD, as supported by the data shown in Figures 4A–4D (Figure 5G, step 4). MLKL is then recruited to the plasma membrane, where TAM kinases phosphorylate MLKL at Tyr376 (Figure 5G, step 5), promoting its oligomerization and formation of membrane-rupturing pores that result in necrotic cell death (Figure 5G, step 6).

Figure 5. TAM Kinases Are Essential for TNF-α and zVAD.fmk-Mediated Systemic Inflammatory Response Syndrome (SIRS) and Phosphorylation of MLKL

(A) Effect of TAM kinase knockout on lethality of mice due to TNF-α + zVAD.fmk (TZ)-induced SIRS. Axl$^{+/-}$ mice are partially protected, while Tyro3$^{-/-}$Axl$^{-/-}$Mertk$^{-/-}$ mice are fully resistant (***p < 0.005 and **p < 0.05, one-way ANOVA). The experiment was done three times, and the data were pooled before plotting and statistical analysis.

(B) Changes in body surface temperatures for mice in (A). The experiment was done three times, and the data were pooled before plotting and statistical analysis. *p < 0.05, **p < 0.01, Mean values ± SEM are shown.

(C) TAM kinase knockout blocks tyrosine phosphorylation of MLKL during SIRS. Liver lysates from wild-type (WT) or Tyro3$^{-/-}$Axl$^{-/-}$Mertk$^{-/-}$ (TKO) mice injected with TZ for 5.5 h were used to immunoprecipitate endogenous MLKL, and pull-downs were immunoblotted with the indicated antibodies.

(D) Effect of TAM kinase inhibition by BMS-777607 (in vivo half-life ~4.5 h) on lethality of mice due to TZ-induced SIRS (**p < 0.05, one-way ANOVA).

(E) Changes in body surface temperatures for mice in (D). *p < 0.05, **p < 0.01, Mean values ± SEM are shown.

(F) TAM kinase inhibition by BMS-777607 blocks tyrosine phosphorylation of MLKL during SIRS. Liver lysates from mice injected with TZ and either vehicle (veh) or BMS-777607 (BMS) for 5.5 h were used to immunoprecipitate endogenous MLKL, and pull-downs were immunoblotted with the indicated antibodies.

(G) Diagram of the mechanistic findings for the TAM-MLKL input into the necroptosis pathway.

(H) Diagram of the oncogenic, anti-inflammatory, and pro-inflammatory inputs from TAM kinases into immunity and cancer.

CellPress

The proposed dual-autoinhibition model of MLKL regulation explains the inability of TAM kinases to interact with MLKL prior to necroptosis activation, despite TAM kinases being constitutively active under basal serum+ conditions (Figures 4A–4C). It is possible that the role of TAM-kinase-mediated phosphorylation of MLKL at Tyr376, in the activation loop of the KD, next to the RIPK3 site Ser358, is to stabilize the active conformation of MLKL primed by the RIPK3-mediation phosphorylation and thus promote oligomer formation via KD-KD interaction. However, the Tyr376 phosphorylation event could also be a signal for recruitment of additional factors that promote MLKL oligomerization or even multimerization or polymerization. How the regulation of MLKL oligomerization by TAM kinases relates to multimerization or polymerization of MLKL (Liu et al., 2017) remains to be elucidated; however, it is likely to be blocked in the absence of TAM kinase input into oligomerization, since multimerization or polymerization of MLKL is downstream of its oligomerization.

The physiological significance of the inhibition of the MLKL-TAM kinase interaction by the 4HB domain and whether it has any effect on the cell-death-independent roles of MLKL remains to be elucidated by knockin studies, where a point mutation in the 4HB domain that disrupts the 4HB-KD interaction without affecting the lipid-binding properties of the 4HB domain would be employed to assess this regulation mechanism at endogenous protein levels.

Notably, a similar model of KD inhibition by a lipid-binding domain has been previously described for Akt, where the PIP$_3$-binding pleckstrin homology (PH) domain of Akt inhibits its KD (Calleja et al., 2007, 2009; Wu et al., 2010), indicating a common kinase regulation mechanism pattern across kinase families, where the lipid-binding domains impinge on the KDs while the molecules are in the cytosol and their inactive state versus their membrane-bound and active state.

Since TAM kinases are important regulators of inflammation and are key for resolution of inflammation, their involvement in regulating necroptosis, a pro-inflammatory cell death type, is of particular interest (Figure 5H). This new function of TAM kinases links them to a widely important subject of inflammation control in cancer, as well as numerous inflammatory diseases, especially those already linked to necroptosis, such as ALS and MS (Ito et al., 2016; Ofengeim et al., 2015). Our studies suggest that TAM kinases represent a unique class of oncoproteins that are anti-apoptotic but pro-necroptotic, suggesting the possible involvement of necroptosis in promoting cancer development.

Epithelial cancer cell lines have been shown to be resistant to necroptosis via loss of RIPK3 expression at the transcriptional regulation level (Koo et al., 2015). TAM kinases are frequently overexpressed in various cancers, and how this overexpression contributes to the resistance of cancer cells to necroptosis is an important question that will be investigated in the future studies. This is especially important in the light of anti-apoptotic nature of these kinases. Whether overexpression of TAM kinases in tumors correlates with increased or decreased sensitivity to necroptosis remains to be investigated.

It is important to note that since TAM kinases are active under normal culture conditions (i.e., in the presence of serum, which contains a TAM ligand called protein S), their activation by nec-

roptosis induction is not necessarily required. Therefore, the kinase-substrate interaction for the TAM-MLKL interaction is likely to be mediated by either spatial regulation or substrate priming and not by kinase activity induction upon necroptosis activation.

Since we employed cell lines that do not express Axl and Mer but express Tyro3, in this study, most of the mechanistic work was done using Tyro3 family member, assuming reported similar kinase specificities and overlapping and/or redundant roles of Tyro3, Axl, and Mer. Moreover, the Tyro3$^{-/-}$Axl$^{+/-}$Mer$^{-/-}$ heterozygous mice were only partially resistant to SIRS (Figure 5A), and Tyro3$^{-/-}$Axl$^{+/-}$Mer$^{-/-}$ MEFs were not fully protected from necroptosis (data not shown), unlike Tyro3$^{-/-}$Axl$^{-/-}$Mer$^{-/-}$ MEFs, suggesting that both Axl and Tyro3 play a role in necroptosis. Due to chromosomal linkage with Tyro3, Mer$^{+/-}$ mice could not be obtained. However, it is possible that a certain isoform-specific regulation in the context of necroptosis might exist, depending on the cell type or tissue type, as most kinase families show redundancy in some biological contexts and divergence in function in others.

In conclusion, this novel role of TAM kinases in promoting necroptosis opens insights into understanding their function as key regulators of inflammation and provides the first cross-talk between an oncogenic kinase family and necroptosis, which is implicated in cancer (Najafov et al., 2017). This novel pro-necroptosis role of TAM kinases suggests that tumors with overexpression of TAM kinases would be sensitized to necroptosis, and thus, TAM kinase overexpression is a potential necroptosis vulnerability marker for anti-cancer treatments that employ necroptosis induction to shrink tumors.

STAR★METHODS

Detailed methods are provided in the online version of this paper and include the following:

- KEY RESOURCES TABLE
- CONTACT FOR REAGENT AND RESOURCE SHARING
- EXPERIMENTAL CMODEL AND SUBJECT DETAILS
    - Cell Culture
    - Animal Work
- METHOD DETAILS
    - Materials and Antibody Generation
    - Molecular Cloning, CRISPR Knockouts, and siRNA Knockdowns
    - Protein Purification and *In Vitro* Kinase Assays
    - Immunoprecipitation Using Anti-phospho-Tyr376 MLKL Antibody
    - Immunoblotting
    - Cell Death and Survival Assays
    - Microscopy
    - Phosphomapping
- QUANTIFICATION AND STATISTICAL ANALYSIS

SUPPLEMENTAL INFORMATION

Supplemental Information can be found online at https://doi.org/10.1016/j.molcel.2019.05.022.

CellPress

REFERENCES

Beausoleil, S.A., Villén, J., Gerber, S.A., Rush, J., and Gygi, S.P. (2006). A probability-based approach for high-throughput protein phosphorylation analysis and site localization. Nat Biotechnol 24, 1285–1292.

Calleja, V., Alcor, D., Laguerre, M., Park, J., Vojnovic, B., Hemmings, B.A., Downward, J., Parker, P.J., and Larijani, B. (2007). Intramolecular and intermolecular interactions of protein kinase B define its activation in vivo. PLoS Biol 5, e95.

Calleja, V., Laguerre, M., Parker, P.J., and Larijani, B. (2009). Role of a novel PH-kinase domain interface in PKB/Akt regulation: structural mechanism for allosteric inhibition. PLoS Biol 7, e17.

Cho, Y.S., Challa, S., Moquin, D., Genga, R., Ray, T.D., Guildford, M., and Chan, F.K.-M. (2009). Phosphorylation-driven assembly of the RIP1-RIP3 complex regulates programmed necrosis and virus-induced inflammation. Cell 137, 1112–1123.

Christofferson, D.E., and Yuan, J. (2010). Necroptosis as an alternative form of programmed cell death. Curr. Opin. Cell Biol. 22, 263–268.

Declercq, W., Vanden Berghe, T., and Vandenabeele, P. (2009). RIP kinases at the crossroads of cell death and survival. Cell 138, 229–232.

Degterev, A., Huang, Z., Boyce, M., Li, Y., Jagtap, P., Mizushima, N., Cuny, G.D., Mitchison, T.J., Moskowitz, M.A., and Yuan, J. (2005). Chemical inhibitor of nonapoptotic cell death with therapeutic potential for ischemic brain injury. Nat. Chem. Biol. 1, 112–119.

Duprez, L., Takahashi, N., Van Hauwermeiren, F., Vandendriessche, B., Goossens, V., Vanden Berghe, T., Declercq, W., Libert, C., Cauwels, A., and Vandenabeele, P. (2011). RIP kinase-dependent necrosis drives lethal systemic inflammatory response syndrome. Immunity 35, 908–918.

Eid, S., Turk, S., Volkamer, A., Rippmann, F., and Fulle, S. (2017). KinMap: A web-based tool for interactive navigation through human kinome data. BMC Bioinformatics 18, 16.

He, S., Wang, L., Miao, L., Wang, T., Du, F., Zhao, L., and Wang, X. (2009). Receptor interacting protein kinase-3 determines cellular necrotic response to TNF-alpha. Cell 137, 1100–1111.

Hildebrand, J.M., Tanzer, M.C., Lucet, I.S., Young, S.N., Spall, S.K., Sharma, P., Pierotti, C., Garnier, J.-M., Dobson, R.C.J., Webb, A.I., et al. (2014). Activation of the pseudokinase MLKL unleashes the four-helix bundle domain

to induce membrane localization and necroptotic cell death. Proc. Natl. Acad. Sci. USA 111, 15072–15077.

Hitomi, J., Christofferson, D.E., Ng, A., Yao, J., Degterev, A., Xavier, R.J., and Yuan, J. (2008). Identification of a molecular signaling network that regulates a cellular necrotic cell death pathway. Cell 135, 1311–1323.

Hornbeck, P.V., Zhang, B., Murray, B., Kornhauser, J.M., Latham, V., and Skrzypek, E. (2015). PhosphoSitePlus, 2014: mutations, PTMs and recalibrations. Nucleic Acids Res 43, D512–D520.

Hoxhaj, G., Najafov, A., Toth, R., Campbell, D.G., Prescott, A.R., and MacKintosh, C. (2012). ZNRF2 is released from membranes by growth factors and, together with ZNRF1, regulates the Na+/K+ATPase. J. Cell Sci. 125, 4662–4675.

Ito, Y., Ofengeim, D., Najafov, A., Das, S., Saberi, S., Li, Y., Hitomi, J., Zhu, H., Chen, H., Mayo, L., et al. (2016). RIPK1 mediates axonal degeneration by promoting inflammation and necroptosis in ALS. Science 353, 603–608.

Janssen, J.W., Schulz, A.S., Steenvoorden, A.C., Schmidberger, M., Strehl, S., Ambros, P.F., and Bartram, C.R. (1991). A novel putative tyrosine kinase receptor with oncogenic potential. Oncogene 6, 2113–2120.

Kaiser, W.J., Sridharan, H., Huang, C., Mandal, P., Upton, J.W., Gough, P.J., Sehon, C.A., Marquis, R.W., Bertin, J., and Mocarski, E.S. (2013). Toll-like receptor 3-mediated necrosis via TRIF, RIP3, and MLKL. J. Biol. Chem. 288, 31268–31279.

Koo, G.-B., Morgan, M.J., Lee, D.-G., Kim, W.-J., Yoon, J.-H., Koo, J.S., Kim, S.I., Kim, S.J., Son, M.K., Hong, S.S., et al. (2015). Methylation-dependent loss of RIP3 expression in cancer represses programmed necrosis in response to chemotherapeutics. Cell Res. 25, 707–725.

Lai, C., Gore, M., and Lemke, G. (1994). Structure, expression, and activity of Tyro 3, a neural adhesion-related receptor tyrosine kinase. Oncogene 9, 2567–2578.

Lemke, G. (2013). Biology of the TAM receptors. Cold Spring Harb. Perspect. Biol. 5, a009076.

Lemke, G., and Rothlin, C.V. (2008). Immunobiology of the TAM receptors. Nat. Rev. Immunol. 8, 327–336.

Li, J., McQuade, T., Siemer, A.B., Napetschnig, J., Moriwaki, K., Hsiao, Y.-S., Damko, E., Moquin, D., Walz, T., McDermott, A., et al. (2012). The RIP1/RIP3 necrosome forms a functional amyloid signaling complex required for programmed necrosis. Cell 150, 339–350.

Linger, R.M.A., Keating, A.K., Earp, H.S., and Graham, D.K. (2008). TAM receptor tyrosine kinases: biologic functions, signaling, and potential therapeutic targeting in human cancer. Adv. Cancer Res. 100, 35–83.

Liu, S., Liu, H., Johnston, A., Hanna-Addams, S., Reynoso, E., Xiang, Y., and Wang, Z. (2017). MLKL forms disulfide bond-dependent amyloid-like polymers to induce necroptosis. Proc. Natl. Acad. Sci. USA 114, E7450–E7459.

Lu, Q., and Lemke, G. (2001). Homeostatic regulation of the immune system by receptor tyrosine kinases of the Tyro 3 family. Science 293, 306–311.

Lu, J., Bai, L., Sun, H., Nikolovska-Coleska, Z., McEachern, D., Qiu, S., Miller, R.S., Yi, H., Shangary, S., Sun, Y., et al. (2008). SM-164: a novel, bivalent Smac mimetic that induces apoptosis and tumor regression by concurrent removal of the blockade of cIAP-1/2 and XIAP. Cancer Res. 68, 9384–9393.

Manning, G., Whyte, D.B., Martinez, R., Hunter, T., and Sudarsanam, S. (2002). The protein kinase complement of the human genome. Science 298, 1912–1934.

Murphy, J.M., Czabotar, P.E., Hildebrand, J.M., Lucet, I.S., Zhang, J.-G., Alvarez-Diaz, S., Lewis, R., Lalaoui, N., Metcalf, D., Webb, A.I., et al. (2013). The pseudokinase MLKL mediates necroptosis via a molecular switch mechanism. Immunity 39, 443–453.

Murphy, J.M., Lucet, I.S., Hildebrand, J.M., Tanzer, M.C., Young, S.N., Sharma, P., Lessene, G., Alexander, W.S., Babon, J.J., Silke, J., et al. (2014). Insights into the evolution of divergent nucleotide-binding mechanisms among pseudokinases revealed by crystal structures of human and mouse MLKL. Biochem. J. 457, 369–377.

Najafov, J., and Najafov, A. (2017). CrossCheck: an open-source web tool for high-throughput screen data analysis. Sci. Rep. 7, 5855.

Najafov, A., Sommer, E.M., Axten, J.M., Deyoung, M.P., and Alessi, D.R. (2011). Characterization of GSK2334470, a novel and highly specific inhibitor of PDK1. Biochem. J. *433*, 357–369.

Najafov, A., Chen, H., and Yuan, J. (2017). Necroptosis and cancer. Trends Cancer *3*, 294–301.

Newton, K., Dugger, D.L., Maltzman, A., Greve, J.M., Hedehus, M., Martin-McNulty, B., Carano, R.A.D., Cao, T.C., van Bruggen, N., Bernstein, L., et al. (2016). RIPK3 deficiency or catalytically inactive RIPK1 provides greater benefit than MLKL deficiency in mouse models of inflammation and tissue injury. Cell Death Differ. *23*, 1565–1576.

Ofengeim, D., Ito, Y., Najafov, A., Zhang, Y., Shan, B., DeWitt, J.P., Ye, J., Zhang, X., Chang, A., Vakifahmetoglu-Norberg, H., et al. (2015). Activation of necroptosis in multiple sclerosis. Cell Rep. *10*, 1836–1849.

Paolino, M., Choidas, A., Wallner, S., Pranjic, B., Uribesalgo, I., Loeser, S., Jamieson, A.M., Langdon, W.Y., Ikeda, F., Fededa, J.P., et al. (2014). The E3 ligase Cbl-b and TAM receptors regulate cancer metastasis via natural killer cells. Nature *507*, 508–512.

Pasparakis, M., and Vandenabeele, P. (2015). Necroptosis and its role in inflammation. Nature *517*, 311–320.

Rickard, J.A., O'Donnell, J.A., Evans, J.M., Lalaoui, N., Poh, A.R., Rogers, T., Vince, J.E., Lawlor, K.E., Ninnis, R.L., Anderton, H., et al. (2014). RIPK1 regulates RIPK3-MLKL-driven systemic inflammation and emergency hematopoiesis. Cell *157*, 1175–1188.

Rothlin, C.V., Ghosh, S., Zuniga, E.I., Oldstone, M.B.A., and Lemke, G. (2007). TAM receptors are pleiotropic inhibitors of the innate immune response. Cell *131*, 1124–1136.

Schroeder, G.M., An, Y., Cai, Z.-W., Chen, X.-T., Clark, C., Cornelius, L.A.M., Dai, J., Gullo-Brown, J., Gupta, A., Henley, B., et al. (2009). Discovery of N-(4-(2-amino-3-chloropyridin-4-yloxy)-3-fluorophenyl)-4-ethoxy-1-(4-fluorophenyl)-2-oxo-1,2-dihydropyridine-3-carboxamide (BMS-777607), a selective and orally efficacious inhibitor of the Met kinase superfamily. J. Med. Chem. *52*, 1251–1254.

Silke, J., Rickard, J.A., and Gerlic, M. (2015). The diverse role of RIP kinases in necroptosis and inflammation. Nat. Immunol. *16*, 689–697.

Sun, L., d Wang, H., Wang, Z., He, S., Chen, S., Liao, D., Wang, L., Yan, J., Liu, W., Lei, X., and Wang, X. (2012). Mixed lineage kinase domain-like protein mediates necrosis signaling downstream of RIP3 kinase. Cell *148*, 213–227.

Tait, S.W.G., and Green, D.R. (2008). Caspase-independent cell death: leaving the set without the final cut. Oncogene *27*, 6452–6461.

Tang, Y., Wu, S., Liu, Q., Xie, J., Zhang, J., Han, D., Lu, Q., and Lu, Q. (2015). Mertk deficiency affects macrophage directional migration via disruption of cytoskeletal organization. PLoS ONE *10*, e0117787.

Tanzer, M.C., Tripaydonis, A., Webb, A.I., Young, S.N., Varghese, L.N., Hall, C., Alexander, W.S., Hildebrand, J.M., Silke, J., and Murphy, J.M. (2015). Necroptosis signalling is tuned by phosphorylation of MLKL residues outside the pseudokinase domain activation loop. Biochem. J. *471*, 255–265.

Tanzer, M.C., Matti, I., Hildebrand, J.M., Young, S.N., Wardak, A., Tripaydonis, A., Petrie, E.J., Mildenhall, A.L., Vaux, D.L., Vince, J.E., et al. (2016). Evolutionary divergence of the necroptosis effector MLKL. Cell Death Differ. *23*, 1185–1197.

Wang, H., Sun, L., Su, L., Rizo, J., Liu, L., Wang, L.-F., Wang, F.-S., and Wang, X. (2014). Mixed lineage kinase domain-like protein MLKL causes necrotic membrane disruption upon phosphorylation by RIP3. Mol. Cell *54*, 133–146.

Waterhouse, A.M., Procter, J.B., Martin, D.M.A., Clamp, M., and Barton, G.J. (2009). Jalview Version 2—a multiple sequence alignment editor and analysis workbench. Bioinformatics *25*, 1189–1191.

Wu, W.I., Voegtli, W.C., Sturgis, H.L., Dizon, F.P., Vigers, G.P.A., and Brandhuber, B.J. (2010). Crystal structure of human AKT1 with an allosteric inhibitor reveals a new mode of kinase inhibition. PLoS ONE *5*, e12913.

Yuan, J., and Kroemer, G. (2010). Alternative cell death mechanisms in development and beyond. Genes Dev. *24*, 2592–2602.

Zhang, D.-W., Shao, J., Lin, J., Zhang, N., Lu, B.-J., Lin, S.-C., Dong, M.-Q., and Han, J. (2009). RIP3, an energy metabolism regulator that switches TNF-induced cell death from apoptosis to necrosis. Science *325*, 332–336.

CellPress

STAR★METHODS

KEY RESOURCES TABLE

REAGENT or RESOURCE	SOURCE	IDENTIFIER
Antibodies		
Anti-RIPK3	Abcam	ab56164; RRID:AB_2178667
Anti-phospho-hMLKL (S358)	Abcam	ab187091; RRID:AB_2619685
Anti-hMLKL	Abcam	ab183770
Anti-Tyro3	Cell Signaling	#5585; RRID:AB_10706782
Anti-Axl	Cell Signaling	#4939; RRID:AB_823432
Anti-Mer	Cell Signaling	#4319; RRID:AB_10614528
Anti-RIPK1	Cell Signaling	#3493; RRID:AB_2305314
Anti-phospho-RIPK3 (Ser227)	Cell Signaling	#93654; RRID:AB_2800206
Anti-phospho-RIPK1 (Ser166)	Cell Signaling	#65746; RRID:AB_2799693
Anti-IKKβ (D30C6)	Cell Signaling	#8943; RRID:AB_11024092
Anti-phospho-hMLKL (Y376)	In house	NA
Anti-MLKL	In house	NA
Anti-phospho-tyrosine, clone 4G10®	Millipore	05-321; RRID:AB_309678
Anti-IkBa	Santa Cruz Biotechnology	sc-371
Anti-Actin	Santa Cruz Biotechnology	sc-1615; RRID:AB_630835
Anti-Tubulin	Sigma	T-9026; RRID:AB_477593
Chemicals, Peptides, and Recombinant Proteins		
TNFa	Cell Sciences	CRT192C
Tet System Approved FBS 500 mL	Clontech	631106
DMEM medium	Corning	10-017-CV
FLAG-mTNF	Enzo Life Sciences	ALX-522-009-C050
Glutathione Sepharose 4B	GE Healthcare	17-0756-01
McCoy's 5A medium	GIBCO	16600-082
SM-164	In house	NA
PEI MAX (MW 40,000)	Polysciences	24765
Amphotericin B	Santa Cruz Biotechnology	sc-202462A
BMS-777607	SelleckChem	S1561
LDC1267	SelleckChem	S7638
Hygromycin B	Sigma	H3274-50MG
Blasticidine S hydrochloride	Sigma	15205-25MG
ATP solution (100mM)	Sigma	A6559
zVAD.fmk	Sigma	V116
Anti-FLAG M2 Affinity Gel	Sigma	A2220
3X FLAG® Peptide	Sigma	F4799
Mouse TrueBlot® ULTRA	Rockland	18-8817-31
Rabbit TrueBlot®	Rockland	18-8816-31
Lipofectamine RNAiMAX	Thermo Scientific	13778-150
ProLong® Diamond Antifade Mountant with DAPI	Thermo Scientific	P36966
HEPES (1M, pH 7.4)	Thermo Scientific	15630080
Necrosulfonamide	Tocris	5025
Critical Commercial Assays		
Toxilight	Lonza	LT07-117
CellTiterGlo®	Promega	G7571

(*Continued on next page*)

CellPress

Continued

REAGENT or RESOURCE	SOURCE	IDENTIFIER
Plasmid Maxi Kit	QIAGEN	12162
SuperSep Phos-tag gels	Wako Chemicals USA	198-17981
Experimental Models: Cell Lines		
HT-29 cells	ATCC	HTB-38
HEK293T cells	ATCC	CRL-11268
HEK293-FlpIn-Trex cells	Thermo Scientific	R78007
FADD-deficient Jurkat cells	Gift from John Blenis	
Primary MEFs	In house	NA
MLKL−/− MEFs	Gift from	NA
HeLa-FlpIn-Trex cells	Thermo Scientific	R71407
L929 cells	ATCC	CCL-1
iBMDM cells	In house	NA
Experimental Models: Organisms/Strains		
Tyro3−/−Axl−/−Mertk−/− mice	Gift from Dr. Qingxian Lu	NA
C57BL/6N mice	Taconic Biosciences	B6NTac
Oligonucleotides		
[h/m]Tyro3 siRNA-1	GenePharma	GCAGACGCCAUAUGCUGGCAUUGAA
[h/m]Tyro3 siRNA-2	GenePharma	AACAAGUUUGGCCACGUGUGGAUGG
hTyro3 sgRNA	Integrated DNA Technologies	GACAGTGTCTCAGGGGCAGC
hMLKL sgRNA	Integrated DNA Technologies	CGTCTAGGAAACCGTGTGCA
Recombinant DNA		
pSpCas9(BB)-2A-Puro (pX459)	Addgene	#62988
pLenti-SV40 Large+small T-antigen	Addgene	#22298
pcDNA3.1	Thermo Scientific	V79020
pCDNA5.5/FRT/TO	Thermo Scientific	V652020
pOGT44	Thermo Scientific	V600520
Software and Algorithms		
Venny	NA	http://bioinfogp.cnb.csic.es/tools/venny/index.html
CrossCheck	Najafov and Najafov, 2017	http://www.proteinguru.com/crosscheck/
GraphPad Prism v7.0	NA	https://www.graphpad.com/

CONTACT FOR REAGENT AND RESOURCE SHARING

Further information and requests for reagents may be directed to and will be fulfilled by the Lead Contact, Junying Yuan (jyuan@hms.harvard.edu).

EXPERIMENTAL CModel AND SUBJECT DETAILS

Cell Culture

HEK293T, L929 and MEF cells were grown in DMEM medium (Corning, 10-017-CV, with L-glutamine, with 4.5 g/L glucose, without pyruvate); HT-29 cells were grown in McCoy's 5A medium (GIBCO, 16600-082, with L-glutamine); FADD-deficient Jurkat cells were grown in RPMI medium (Corning, 10-040-CV, with L-glutamine). These media were supplemented with 10% FBS (Sigma), 1X penicillin/streptomycin (Life Technologies) and 1 μg/ml amphotericin B (Santa Cruz Biotechnology, sc-202462A). Doxycycline-inducible isogenic HEK293 stable cell lines were generated by co-transfecting the parental HEK293-Flp-In™-T-REx™ cell line (Life Technologies) with pcDNA5-FRT-TO plasmids of interest and pOG44 Flp recombinase plasmid at 1:9 ratio, using PEI MAX (MW 40,000, Polysciences, 24765) and selecting with 100 μg/ml hygromycin (Sigma, H3274) and 2.5 μg/ml Blasticidine S (Sigma, 15205). These cells were always grown in DMEM medium supplemented with 10% Tet System Approved FBS (Clontech, 631106) and penicillin/streptomycin. TAM knockout MEFs were described previously (Tang et al., 2015). Primary MEFs were immortalized by transfection with SV40 Large+small antigen plasmid (Addgene, 22298).

Animal Work

C57BL/6J mice were purchased from Taconic Biosciences. Mice were maintained in a pathogen-free environment. Experiments were conducted according to the protocols approved by the Harvard Medical School Animal Care Committee. TNFα+zVAD injections were performed as previously described (Duprez et al., 2011). Mice aged 8-14 weeks were given intraperitoneal injections of zVAD.fmk 15min before (10 μg / g mouse weight dose) and 1hr after (4 μg/g mouse weight dose) an intravenous (tail vein) TNFα injection (0.36 μg / g weight mouse). Vehicle control (4% DMSO + 45% PEG 300 + 5% Tween 80) or BMS-777607 dissolved in the vehicle solution were injected at 20 mg/kg dose at the time of the first zVAD.fmk injection. Mouse survival was monitored at 30min intervals and scored. Mouse body surface temperature was monitored using and Etekcity ETC 8250 Non-contact Digital IR Infrared Thermometer.

METHOD DETAILS

Materials and Antibody Generation

BMS-777607 and LDC1267 were purchased from SelleckChem. Protein A/G-Sepharose and Glutathione-Sepharose were purchased from Pierce. [γ-^{32}P] ATP was from Perkin-Elmer. Luminol (A8511), p-coumaric acid (C9008), Tween 20, anti-Flag M2 agarose beads, Na_3VO_4 were from Sigma. DMSO (sc-20258) was from Santa Cruz Biotechnology. Lipofectamine 2000 was from Life Technologies. The following antibodies were used in this study: Tyro3 (Cell Signaling Technology (CST, #5585); Axl (CST, #4939); Mer (CST, #4319); RIPK1 (CST, #3493); p-RIPK1 Ser166 (CST, #65746); GAPDH (CST, #5174); mRIPK3 (Serotec/Biorad, AHP1797); hRIPK3 (Abcam, ab56164); mMLKL (Sigma, SAB1302339); p-MLKL (S358) (Abcam, ab187091); hMLKL (Abcam, ab183770), Anti-Phosphotyrosine Antibody, clone 4G10® (Millipore, 05-321); Anti-Tubulin (Sigma, T9026); beta-actin (Santa Cruz Biotechnologies, sc-81178). Polyclonal rabbit anti-MLKL phospho-Tyr376 antibody was raised against CKTDRVKSTA-pY-LSPQE peptide and purified using protein A/G-Sepharose beads, following a 10-minute elution with 0.1M glycine pH 3.5 and immediate neutralization with 100 mM HEPES, pH7.4. Monoclonal antibodies against RIPK3 and MLKL were generated using standard methods after immunizing mice with purified recombinant protein fragments. Mouse MLKL fragment spanning amino acids 112-433 and human RIPK3 fragment spanning amino acids 248-518 were used. Stocks of 200 mM Na_3VO_4 were prepared by several cycles of boiling and adjusting the pH of the solution to 10, until the solution became clear. The stocks were then stored in single-use aliquots at $-20°C$.

Molecular Cloning, CRISPR Knockouts, and siRNA Knockdowns

RNA was isolated from HEK293 and HeLa cells using RNeasy kit (QIAGEN) and cDNA synthesis was performed using SuperScript II Reverse Transcriptase (Life Technologies) or using RNA to cDNA EcoDry Premix (Double Primed) (Takara Bio). Molecular cloning was performed using New England Biolabs restriction enzymes and T4 DNA ligase. Plasmids were transformed into in-house-generated chemically-competent DH5α E. coli cells. Plasmid purifications and extractions were performed using QIAprep Spin Miniprep Kit (QIAGEN) and QIAquick Gel Extraction Kit (QIAGEN). sgRNA sequences, used for generation of CRISPR/Cas9-mediated knockout cell lines, were cloned into pX459-puro vector (Addgene). sgRNA sequences were hTyro3: GACAGTGTCTCAGGGGCAGC; hMLKL: CGTCTAGGAAACCGTGTGCA. HT-29 cells were transfected with pX459-puro-sgRNA plasmids using Lipofectamine 2000, according to manufacturer's protocol, and 48 hours post-transfection were switched to McCoy's medium containing 2 μg/ml puromycin, for 7 days. Individual clones were picked and analyzed by western blotting and sequencing for loss of expression and in-dels, respectively. Sequencing reactions were carried out with an ABI3730xl DNA analyzer at the DNA Resource Core of Dana-Farber/Harvard Cancer Center (funded in part by NCI Cancer Center support grant 2P30CA006516-48). Lipofectamine RNAiMAX (Life Technologies) was used for transfection of siRNA as per manufacturer's protocol. Tyro3 siRNA oligos used for knockdown experiments were: GCAGACGCCAUAUGCUGGCAUUGAA and AACAAGUUUGGCCACGUGUGGAUGG.

Protein Purification and *In Vitro* Kinase Assays

In vitro kinase assays were performed as previously described (Najafov et al., 2011). pcDNA3.1-hTyro3-Flag and pEBG-hMLKL-Flag plasmids were transfected into HEK293T cells at 50% confluency in 1-day-old medium (transfection per 15cm dish: 20 μg plasmid + 55 μl PEI + 1ml OptiMEM, incubate for 20 min at RT) and expressed for 48 hr. Cells were lyzed in 0.75 mL of NP-40 lysis buffer (NLB) (25 mM HEPES (pH 7.5), 0.2% NP-40, 120 mM NaCl, 0.27 M sucrose, 2 mM EDTA, 2 mM EGTA, 50 mM NaF, 10 mM beta-glycerophosphate, 5 mM Na- pyrophosphate, 5 mM Na-orthovanadate (added fresh), 0.1% BME (added fresh), 1mM PMSF (added fresh), 2X Complete protease inhibitor cocktail (Roche, added fresh)). For GST-hMLKL-Flag purification cells were lyzed in the NLB lacking the phosphatase inhibitors (EDTA, EGTA, NaF, beta-glycerophosphate, Na-pyrophosphate and Na-orthovanadate). hTyro3-Flag was immobilized on anti-Flag-M2 agarose beads (Sigma) and kinase assays were performed with purified GST-hMLKL-Flag at 30°C for 1.5 hr with 1200 rpm agitation, in the presence of 200 μM of cold ATP and 2 μCi [γ-^{32}P] ATP, 25 mM HEPES (pH 7.5), 1mM NaF, 10mM b-glycerophosphate, 1 mM EGTA, 1X Complete protease inhibitor cocktail (Roche), 1 mM Na-orthovanadate, 10 mM $MnCl_2$, 10 mM MgAcetate and 0.1 mg/ml BSA. For purification of hMLKL-Flag (C-terminally-tagged) pcDNA3.1-hMLKL-Flag plasmid was used and the proteins were bound to anti-Flag-M2 agarose beads for 2hrs on a rotating wheel at 4°C. The beads for both kinase and substrate purification steps were washed twice with NLB containing phosphatase inhibitors (each wash for 5min on a rotating wheel at 4°C) and twice with a wash buffer containing 1% Triton X-100, 250 mM NaCl, 25mM HEPES

pH7.4. GST-tagged proteins were eluted with 20mM gluthathione for 20min at 25°C. Flag-tagged proteins were eluted with 0.1M glycine pH 3.5 for 10min at 25°C and neutralized with 100mM HEPES pH 7.4.

Immunoprecipitation Using Anti-phospho-Tyr376 MLKL Antibody

Cells were lyzed in a Triton X-100-based TLB buffer (25 mM HEPES (pH 7.5), 0.5% Triton X-100, 120 mM NaCl, 0.27 M sucrose, 5 mM EDTA, 5 mM EGTA, 50 mM NaF, 10 mM b-glycerophosphate, 5 mM sodium pyrophosphate, 5 mM Na_3VO_4 (fresh), 0.1% BME, 1mM PMSF (fresh), 2X Complete protease inhibitor cocktail (Thermo)) and immunoprecipitations were performed at 1:100 dilution ratio for 24hrs, on a shaker at 1200rpm, 4°C. Protein A/G-Sepharose beads were added and the immunoprecipitations were continued on a rotating wheel for 2hrs at 4°C. The beads were washed three times with the TLB, 5min each wash, on a rotating wheel at 4°C.

Immunoblotting

Total cell lysates (20-30 μg) or pull-down samples were heated at 70°C for 10 min in 1-1.5X SDS-PAGE sample buffer, subjected to 8%–10% SDS-PAGE and then electrotransferred onto nitrocellulose membranes for 2hrs at 0.4A current with the wet transfer tank submerged in an ice bath. Membranes were blocked for 1 h in TBST buffer containing 10% (w/v) skimmed milk and probed with the indicated antibodies in TBST containing 5% (w/v) BSA for 16 h at 4°C. Detection was performed using HRP-conjugated secondary antibodies, which were diluted in TBST. For detection of MLKL in immunoprecipitation experiments, TrueBlot secondary antibodies (Rockland Immunochemicals Inc., #18-8817-31, #18-8816-31) were employed to avoid interference with heavy chains. In-house-made chemiluminescence reagent (2.5 mM luminol, 0.4 mM p-coumaric acid, 100 mM Tris-HCl, pH 8.6, 0.018% H_2O_2), with which membranes were incubated for 2 min at 25°C before exposure to film and development. SuperSep Phos-tag gels (cat# 198-17981) were purchased from Wako Chemicals USA and used as per manufacturer's protocol.

Cell Death and Survival Assays

Cells were pre-treated with kinase inhibitors Nec-1 s or BMS-777607 at 10 μM final concentration for 30min. For L929 cells, necroptosis was induced by treatment with either 20 ng/ml mouse TNFα, 20 μM zVAD, or combination of both. For MEFs and HT-29 cells, necroptosis was induced by TSZ treatment, which is a combination of 20 ng/ml hTNFα, 0.2 μM SM-164 (30 min pre-treatment) and 20-30 μM zVAD (30 min pre-treatment) or TCZ treatment, which is a combination of 20 ng/ml hTNFα, 0.5-1 μg/ml cycloheximide (30 min pre-treatment), and 20-30 μM zVAD (30 min pre-treatment). ToxiLight Non-destructive Cytotoxicity BioAssay (Lonza, LT07-117) was used for membrane permeabilization cell death assays (for proof-of-principle of lytic cell death), as per manufacturer's instructions. CellTiter-Glo® Luminescent Cell Viability Assay (Promega, G7570) was used to determine cell viability, as per manufacturer's instructions.

Microscopy

All the microscopy was performed at The Nikon Imaging Center at Harvard Medical School, as described previously (Hoxhaj et al., 2012). Briefly, TSZ ± 10 μM BMS-777607 treated cells were fixed with 4% paraformaldehyde and mounted using ProLong® Diamond Antifade Mountant (Thermo). Immunofluorescence for p-hMLKL Ser358 was performed as described previously (Wang et al. 2014).

Phosphomapping

To map Tyro3 phosphosites in MLKL, *in vitro* kinase reactions using cold ATP ± 3 μM BMS-777607 or IP-Flag immunoprecipitates after TSZ (5.5hrs) ± 10 μM BMS-777607 treatment of MLKL^{KO} HT-29 cells stably expressing hMLKL-Flag (at near-endogenous levels) were resolved by 10% SDS-PAGE and proteins were stained with Coomassie stain (0.05% Coomassie Brilliant Blue R, 25% Methanol, 10% Acetic acid). MLKL bands were excised and in-gel trypsin digestion, LC-MS/MS and data analysis were performed as at Taplin Mass Spectrometry Facility, Harvard Medical School. LTQ Orbitrap Velos Pro ion-trap mass spectrometer (Thermo Fisher Scientific, San Jose, CA) and Sequest (ThermoFinnigan, San Jose, CA) software program were used. The modification of 79.9663 mass units to serine, threonine, and tyrosine was included in the database searches to determine phosphopeptides. Phosphorylation assignments were done using the A-score algorithm (Beausoleil et al., 2006).

QUANTIFICATION AND STATISTICAL ANALYSIS

For all experiments, unless otherwise indicated, n was at least 3. Statistical analyses were performed with GraphPad Prism 7 or Microsoft Excel. Data were analyzed with a one-way analysis of variance (ANOVA) test with Bonferroni post-test for non-paired datasets. Student's t test was used for paired datasets. Data points are shown as means ± SEM. Survival curves were analyzed with a log-rank Mantel-Cox test.

Bioinformatics analysis of the genome-wide siRNA screen results from Hitomi et al. was done with ontological information retrieved from Uniprot. The cross-referencing of gene symbol lists was done with CrossCheck (http://www.proteinguru.com/crosscheck) (Najafov and Najafov, 2017) and Venny (http://bioinfogp.cnb.csic.es/tools/venny/index.html). Amino acid sequence alignments were done with Jalview (Waterhouse et al., 2009). Kinome tree analysis was done at Kinhub.org (Eid et al., 2017). Pathway models were drawn in Adobe Fireworks.